УДК 539.171

ELASTIC SCATTERING OF A SECONDARY ^{11}Li BEAM ON ^{28}Si AT 29 MeV/n

F.A.Gareev, S.N.Ershov, G.S.Kazacha, S.M.Lukyanov,
Yu.E.Penionzhkevich, N.K.Skobelev, S.P.Tretyakova
JINR, P.O.Box 79, Dubna, Russia

M.Lewitowicz, C.Borcea, F.Carstoiu, M.G.Saint-Laurent,
A.Kordyasz, R.Anne, P.Roussel-Chomaz
GANIL, BP 5027, F-14021 Caen, France

R.Bimbot, V.Borrel, S.Dogny, D.Guillemaud-Mueller,
A.C.Mueller, F.Pougheon
IPN, F-91406 Orsay, France

Z.Dlouhy, L.Nosek, J.Svanda
Nucl.Phys.Inst., CS-25068 Rez, Chechoslovakia

The elastic scattering of a secondary ^{11}Li beam (29 MeV/n) on a ^{28}Si target has been measured for the first time. To compensate for the low intensity of the secondary beam, an efficient detecting system permitting to obtain reliable experimental data has been used. An attempt has been made to reproduce the data in a phenomenological analysis and with coupled-channel calculations with a double folding optical potentials, with energy and density dependent effective interaction and realistic densities. An unusually large value of the surface diffuseness parameter for the real part is required in the phenomenological optical potential for description of the experimental data. In coupled-channel calculations with the folding optical potential a better description is achieved if a neutron halo of ^{11}Li is taken into account.

The investigation has been performed at the Laboratory of Nuclear Reactions, JINR and GANIL.

Упругое рассеяние вторичного пучка ^{11}Li при 29 МэВ/нуклон на кремнии-28

Ф.А.Гареев и др.

Впервые измерено упругое рассеяние вторичного пучка ^{11}Li (29 МэВ/нуклон) на мишени из ^{28}Si. Для компенсации низкой эффективности вторичного пучка использовалась эффективная детектирующая система, позволявшая получить достоверные экспериментальные данные. Сделана попытка воспроизвести данные с феноменологическим оптическим потенциалом и с использованием потенциала двойной свертки с учетом связанных каналов с энергетической и плотностной зависимостями

эффективного взаимодействия и реалистическими плотностями. Для описания экспериментальных данных феноменологически требуется вводить необычно большое значение параметра поверхностной диффузности реальной части потенциала. В расчетах с использованием связанных каналов с потенциалом двойной свертки лучшее согласие достигается, если брать в учет нейтронное гало в ^{11}Li.

Работа выполнена в Лаборатории ядерных реакций ОИЯИ и ГАНИЛ.

1. Introduction

In recent experiments at GANIL [1], the existing ^{11}Li interaction cross section data [2,21,23] have been complemented by a measurement of the Coulomb dissociation cross section and the neutron angular distribution at an energy of 30 MeV/n. These new data together with measurements of transverse and parallel momentum of ^{9}Li produced in ^{11}Li induced reactions [3,4] have provided further support for the neutron halo hypothesis. Nevertheless, although they give information about the extent of the neutron cloud and the degree of correlation between the two extra-core neutrons, these experiments are unable to provide detailed information about the proton and neutron distributions in ^{11}Li. Such information can, in principle, be obtained from measurements of the elastic-scattering angular distributions. In this way, it should be possible to test various theoretical descriptions of ^{11}Li. The aim of the present experiment was to advance the idea of a «non-destructive» study of ^{11}Li, by measuring its elastic scattering from a ^{28}Si target and to compare it to the elastic scattering of the stable nucleus ^{7}Li.

In the similar measurements performed recently at RIKEN for the ^{9}Li and ^{11}Li nuclei on protons [29] the elastic cross section for the ^{11}Li was found about factor of two smaller than for the ^{9}Li case. However, results of another experiment performed recently at NSCL MSU for the system ^{11}Li + ^{12}C [30] have shown a strong enhancement of the ratio of σ/σ_R for ^{11}Li as compared with the system ^{11}C + ^{12}C. The later observation indicates an enhanced far-side dominance in the angular distribution of the ^{11}Li scattering predicted by Satchler et al. [24]. In the analysis of both the experiments considerable changes in optical potential parameters were necessary to reproduce the ^{11}Li data. In the present work the use of a heavier target should, in principle, enhance the influence of inelastic processes such as break-up and Coulomb excitation of the projectile on the elastic channel.

2. Experimental Method

Secondary beams of 29 MeV/n ^{11}Li (150 pps) and 25.4 MeV/n ^{7}Li (1000 pps) were produced at GANIL in the reaction of a 76 MeV/n ^{18}O pri-

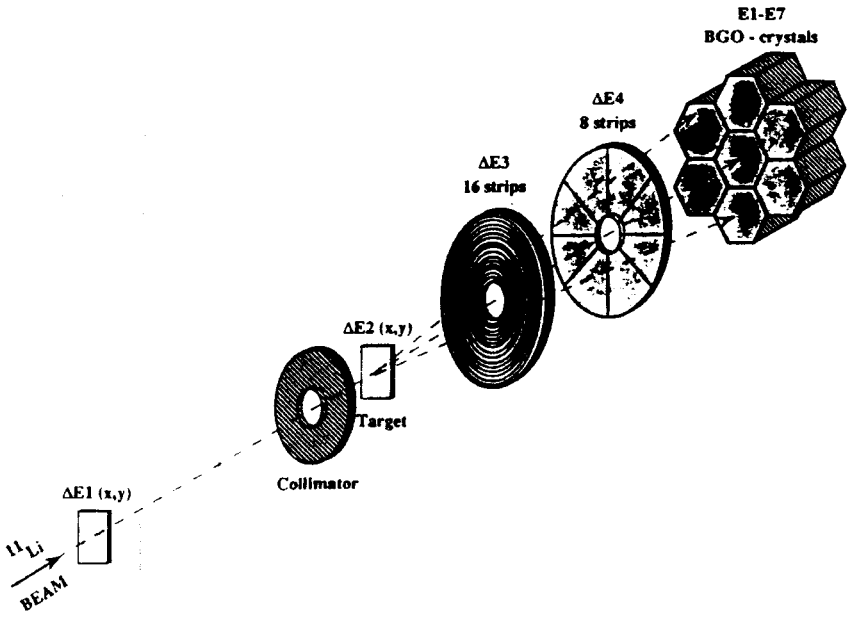

Fig.1. Experimental set-up; see text for details

mary beam bombarding a 360 mg/cm^2 Be + 2900 mg/cm^2 C production target. The outgoing fragments were separated by means of the LISE3 spectrometer [5] and identified by their energy loss and time of flight. The purity of each of the secondary beams was better than 98%. The energy width of the secondary beam was defined by the momentum acceptance of the LISE spectrometer which was set to 2.3% in the case of ^{7}Li and to 9.4% in the case of ^{11}Li. The angular dispersion of the secondary beams was smaller than 0.5°.

A schematic view of the set-up used in the present experiment is shown in figure 1.

To compensate for the low intensity of the secondary beams we choose a detection system with a very high efficiency of registration of scattered particles. At the same time a big angular and energy spread of the secondary beams implied measurements of angle and position on a target for each incoming particle.

The trajectory of each particle was reconstructed by means of two position-sinsitive X-Y silicon detectors ($\Delta E1$, $\Delta E2$), with thickness of 71 mg/cm^2 and 104 mg/cm^2, respectively, placed at the final focal point of the spectrometer. The $\Delta E2$ detector was simultaneously used as an active secondary target. The position resolution of each of detectors was 1 mm.

The incident angle of the particles on the secondary target was measured with the accuracy better than 0.5°. The collimator, 13 mm of diameter placed in front of the target, was used to limit the size of the beam spot. Two circular silicon detectors, one with 16 concentric strips ($\Delta E3$) and other with 8 radial sectors ($\Delta E4$) were used to determine the position and energy loss of scattered particles. The detectors had a 69 mm of outside diameter and a central hole 22 mm of diameter. The distance between the secondary target and the circular detectors was adjusted to cover center-of-mass diffusion angles between 5° and 17° for ^{7}Li and between 5° and 22° for ^{11}Li. A matrix of seven BGO crystals [6] ($E1$-$E7$), used to determine the residual energy of each particle complemented the experimental set-up.

The overall relative energy spread of diffused particles including the energy width of the secondary beam, the intrinsic resolution of the detectors and the energy straggling was about 7% for ^{7}Li and 20% for ^{11}Li ions.

The geometrical efficiency of the system was calculated on the event by event basis taking into account the trajectory of the incident particle and the geometry of the strip detectors. The systematic uncertainties in the measured differential cross section introduced by this procedure are smaller than 10%.

3. Results

Angular distributions of elastic scattering of ^{7}Li and ^{11}Li measured in this experiment are shown in figures 2—7. The error bars indicated for the experimental data correspond to the statistical errors.

The use of the thick target, the angular resolution of $\Delta\theta \approx 1.5°$ and the lack of separation between elastic and inelastic scattering resulted in a flattening of the diffractional structure of the spectra.

The measured distributions for ^{7}Li are in the qualitative agreement with measurements at lower projectile energies [26]. It has a shape typical for scattering of stable nuclei in the Frauenhofer diffraction region — the ratio $\sigma/\sigma_{\text{Ruth.}}$ oscillates and decreases with increasing scattering angle. For the case of ^{11}Li the behaviour of experimental data is rather unusual, the ratio $\sigma/\sigma_{\text{Ruth.}}$ is almost constant in the measured range of angles. The $\sigma/\sigma_{\text{Ruth.}}$ lies for ^{11}Li higher than the one observed in an analogous distribution for the elastic scattering of ^{6}Li [27] and ^{9}Be [28] on ^{28}Si at approximately the same energy of relative motion.

4. Optical Model Analysis

4.1. Phenomenological Optical Potential

The analysis of the elastic scattering was carried out in the framework of the conventional optical model by using the standard Wood—Saxon form:

$$U(r) = V_{\text{Coul}}(r) - Vf_V(r) - iWf_W(r),$$

where $f_V(r)=(1+\exp[(r-R_V)/a_V])^{-1}$, $f_W(r)=(1+\exp[(r-R_W)/a_W])^{-1}$, $R_V = r_V A_T^{1/3}$, $R_W = r_W A_T^{1/3}$ and $V_{\text{Coul}}(r)$ is the Coulomb potential of the uniformly charged sphere. The potential parameters V, W, r_V, r_W, a_V and a_W were fitted to the experimental data using the standard χ^2method.

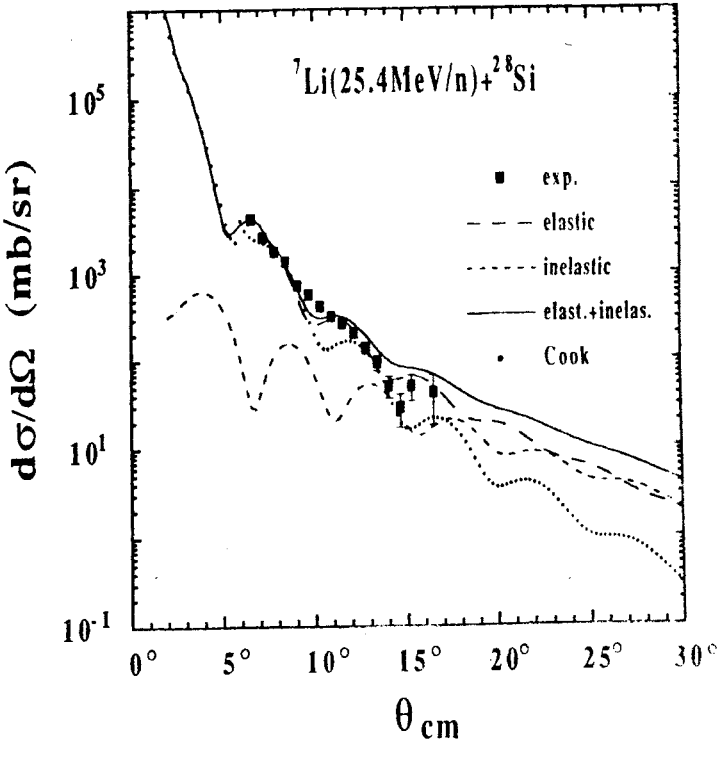

Fig.2. Comparison of the experimental data with theoretical calculations for elastic scattering of ^{7}Li+^{28}Si at energy $E_{^7\text{Li}}$ = 177.8 MeV; long-dashed line — elastic scattering with optical potential «A» from table 1; short-dashed — inelastic cross section; solid — sum of elastic and inelastic cross sections; dotted — elastic cross section with potential from [26]

The theoretical cross sections have been averaged over the angular resolution before comparison to the experimental cross sections.

As the inelastic events have not been resolved by our detection system, we have estimated the inelastic cross section for the excitation of the 2^+, 1.78 MeV state in ^{28}Si and added it incoherently to the elastic one. The estimation of the inelastic cross section was made in the framework of the DWBA. The inelastic form factor was chosen as a derivative of the optical potential:

$$F(r) = \beta_2 R_V \frac{dV(r)}{dr} + i\beta_2 R_W \frac{dW(r)}{dr}$$

with $\beta_2 R_V = \beta_2 R_W = 1.21$ fm [27].

In figure 2 the results of the calculations are compared to the experimental data on the elastic scattering of ^{7}Li. In the calculations the geometric parameters of the optical potential were taken from the global parametrization [26], and the potential depths V and W were adjusted to reproduce the data (see table 1). Theoretical calculations of the elastic scattering are shown by the long dashed line; inelastic one, by the short dashed line; and their sum, by the solid line. For comparison the elastic cross section calculated with parameters from [26] is also shown by the dotted line. From the calculations it follows that the contribution from inelastic processes may be important at the end of the measured angular range and theoretical calculations can describe the experimental data with «standard» optical potentials.

Table 1. Parameters of the optical potentials for the system ^{7}Li + ^{28}Si

	$-V$ MeV	r_V fm	a_V fm	$-W$ MeV	r_W fm	a_W fm	$\langle r_V^2\rangle^{1/2}$ fm	$\langle r_W^2\rangle^{1/2}$ fm	σ_R b	χ^2/N
A	226.8	1.286	0.853	37.26	1.739	0.809	4.38	5.08	1820.	7.0
from [26]	114.2	1.286	0.853	29.75	1.739	0.809	4.38	5.08	1700.	10.4

Table 2. Parameters of the optical potentials for the system ^{11}Li + ^{28}Si

$-V$ MeV	r_V fm	a_V fm	$-W$ MeV	r_W fm	a_W fm	$\langle r_V^2\rangle^{1/2}$ fm	$\langle r_W^2\rangle^{1/2}$ fm	σ_R b	χ^2/N
204.48	0.585	1.737	8.23	2.18	0.425	6.604	5.36	1445.2	1.84

In the case of ^{11}Li the situation is different. The calculations based on the usual nuclear potentials cannot give a reasonable description of the experimental data. As an example, on figure 3 the elastic cross section of ^{11}Li (dotted line) calculated with the optical potential from global paramet-

rization [26] is shown. It is very difficult to give more definite limits for changing the optical potential paramteters based only on the experimental data within a relatively narrow angular range. Therefore, only one example of possible potentials is given in table 2 and the calculated elastic cross section is shown by the long-dashed line in figure 3. The contribution from inelastic scattering, calculated analogously to the ^{7}Li case, is shown by the short-dashed line; and total cross section, by the solid line. The root mean square (rms) radius of the real potential is in our case about 6 fm, and in the strong absorption region the potential has a refractive character. The relatively large value of surface diffuseness of the real part obtained for this potential can reflect the extended density distribution of ^{11}Li. Further important information about the scattering nature may be obtained from a near-side and a far-side decomposition of the elastic cross section [31]. The

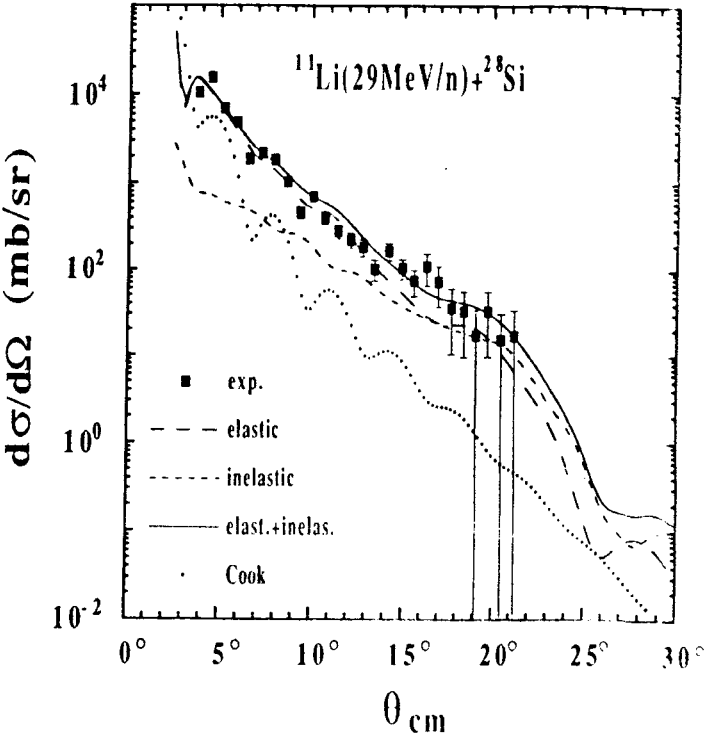

Fig.3. Comparison of the experimental data with theoretical calculations for elastic scattering of ^{11}Li+^{28}Si at energy $E_{^{11}Li}$ = 319 MeV. Long-dashed line — elastic scattering with optical potential from table 2; short-dashed — inelastic cross section; solid — sum of elastic and inelastic cross sections; dotted — elastic cross section with potential from [26]

decomposition for ^{11}Li elastic scattering is shown in Fig.4 where the long-dashed and short-dashed lines give the near-side and far-side contributions, respectively. The crossover point of the near-side and far-side components is close to $\theta \sim 2°$ and the region of diffraction oscillations occupies the angle range up to ~ 8°. At larger angles the far-side component dominates in the elastic cross section. In the case of ^{7}Li scattering the crossover point is near 8° and the region of difraction oscillation spreads up to nearly 20°. Thereby, the smoothness of σ/σ_R in the ^{11}Li case at angles larger than $\theta \geq 10°$ may be connected with a more strong manifestation of nuclear refractive properties in halo nuclei. The elastic cross section for the potential given in table 2 shows the picture of the rainbow scattering [32]. Of course, it does not mean that the rainbow scattering is revealed in ^{11}Li scattering. The appearance of this effect will depend on transparency of nuclear potentials. To give more definite answers, it is necessary to have the experimental data for ^{11}Li scattering in a wider angle interval covered by the exponential fall-off of the elastic cross sections and diffraction oscillations at small angles.

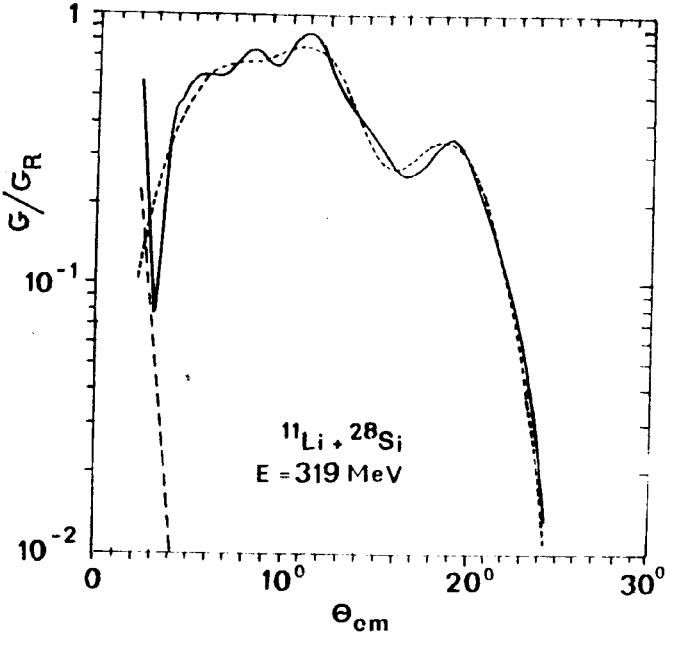

Fig.4. The near-side and far-side decomposition of the elastic scattering ^{11}Li+^{28}Si at energy $E_{^{11}\mathrm{Li}}$ = 319 MeV.Solid line, long-dashed and short-dashed are elastic cross section, near-side and far-side contributions, respectively

The contribution of soft modes in ^{11}Li [33] to the elastic cross section is also possible and requires further investigations.

4.2. Double Folding Potential

Simplified coupled channel (CC) calculations were done using the code ECIS [7]. The ^{28}Si was treated as a rigid rotor and couplings involving both excitation and de-excitation between ground state (0^+) and first excited state (2^+) were used. The $B(E2\uparrow)$ value was taken from the compilation [8] and a deformation length of $\delta = 1.15$ fm was used, which gave satisfactory results in a similar CC calculation for ^{6}Li + ^{28}Si at 210 MeV [9].

The bare CC optical potential (the real part) was calculated in the semi-microscopic double folding model [10] using the density and energy dependent effective interaction (DDM3Y) from [11,12]. The geometry of the imaginary part of the optical potential was taken to be the same as for the real part:

$$V_{\text{opt}}(r) = (N_v + iN_w)V_{\text{DDM3Y}}(r).$$

No attempt has been done to fit the normalization constants N_v, N_w but rather they have been fixed by some physical requirements or by analogy with similar systems. The antisymmetrization effects and the density dependence of the effective interaction in the calculation of the folding potential were treated similarly as in reference [12]. The necessary nuclear densities were constructed by standard Hartree-Fock (H.F.) calculation using Skyrme II (SkII) parametrization of the effective interaction [13]. Spherical symmetry and occupation numbers determined by single particle energies were assumed. The nuclear matter rms radii of the resulted densities (r_m) and the rms radii of the corresponding DDM3Y potentials (r_V) are given in table 3. Also the corresponding values for the «halo» density of Bertsch et al. [14] are indicated. The rms radii of the halo density of Bertsch et al. agree with the effective rms matter radius of 3.12 ± 0.16 fm extracted by Tanihata et al. [15] from the measured interaction cross section at high energy. Therefore it is interesting to check this density in the elastic scattering of ^{11}Li at lower energy.

As a test ground for our calculations, the ^{6}Li elastic scattering on ^{28}Si at 154 MeV [16] was taken. Studies [17—19] on elastic scattering of light Li isotopes in a wide range of energy and targets resulted in a strong renormalization (up to 50%) of the effective M3Y interaction in order to explain the data. It was suggested by Sakuragi [19] that this reduction could be explained by projectile break-up effects. The dynamical polarization potential (DPP) induced by projectile break-up process has a repulsive surface contribution to the real optical potential with a strength of about 40% of the

Table 3. The matter density rms radii for Li isotopes and ^{28}Si calculated with the Hartree-Fock method and the Skyrme II potential $\langle r_m^2\rangle^{1/2}$ and the rms radii of the corresponding DDM3Y folding potentials $\langle r_V^2\rangle^{1/2}$

	^{6}Li	^{7}Li	^{11}Li	^{28}Si
$\langle r_m^2\rangle^{1/2}$ [fm]	2.24[a]	2.31[a]	2.68[a] 2.99[b]	3.1a)
$\langle r_V^2\rangle^{1/2}$ [fm]	4.034[a]	4.083[a]	4.321[a] 4.579[b]	

a) calculated with the standard Hartree-Fock method and the Skyrme II potential [13].
b) calculated with the halo density of Bertsch et al. [14].

Table 4. Effective square radius r_0^2 and total reaction cross sections σ_R for Li isotpes on ^{28}Si

	^{6}Li	^{7}Li	^{8}Li	^{9}Li	^{11}Li
E [MeV/n]	25.7	25.4	25.4	29	29
r_0^2 [fm^2]	1.290[a]	1.285[a]	1.290[a]	1.246[a]	1.305[a]
σ_R [mb]	1577[b]	1672[b]	1768[b]	1771[b]	2001[b]
σ_R [mb]	1521[c]	1583[c]			2064[c] 1402[d]
σ_R [mb]					2947±386[e]

[a] from Saint-Laurent et al. [21],
[b] values calculated for the reactions ^{n}Li+^{28}Si with the formula of Kox et al. [25] and parameters from [21],
[c] calculated with DDM3Y and $N_V = N_W = 1.0$,
[d] calculated with DDM3Y and $N_V = 0.60$, $N_W = 0.18$,
[e] experimental value of Villari et al. [23] at 25.5 MeV/n.

folding potential and a negligible imaginary part, with the effect of decreasing the far-side tail component of the scattering amplitude at large angles. Similar reduction has been found recently in a secondary ^{7}Be beam scattering on ^{12}C at 140 MeV by Yamagata [20]. However, there is no need for such a reduction in the calculations that we performed using DDM3Y effective interaction. The results obtained for ^{6}Li with the normalization N_v = = 1.0, $N_W = 0.9$ (figure 5) show a reasonable agreement with the data.

In a next step, the same procedure was applied for ^{7}Li data measured in the present experiment. As can be seen in figure 5 the incoherent addtion of elastic and inelastic scattering results in a rather flat diffractional pattern.

The calculated reaction cross sections for ^{6,7}Li are in good agreement with the estimated values based on the semiempirical formula of Kox et al. [25] with the parameters from Saint-Laurent et al [21] (see table 4).

In the same spirit, calculations were performed for ^{11}Li elastic scattering data. In contrast to the ^{7}Li case, the experimental ^{11}Li cross section lies above and decreases slower than the corresponding CC prediction if the CC bare optical potential is calculated with the normalization $N_v = 1.0$, $N_W = 1.0$ (figure 6). The H.F.—SkII density for ^{28}Si and the density of Bertsch et al [14] (solid line) and H.F.—SkII (dashed line) for ^{11}Li were used. While the calculated elastic cross section is rather insensitive to the value of the deformation of the potential over the range of experimental data, the inelastic one depends strongly on this parameter. For example, the ratio $(\sigma_{el} + \sigma_{in})/\sigma_{el}$ doubles at large angles (> 15°) when the deformation length is chaged from 1.15 to 1.48 fm. However, in order to bring the calcu-

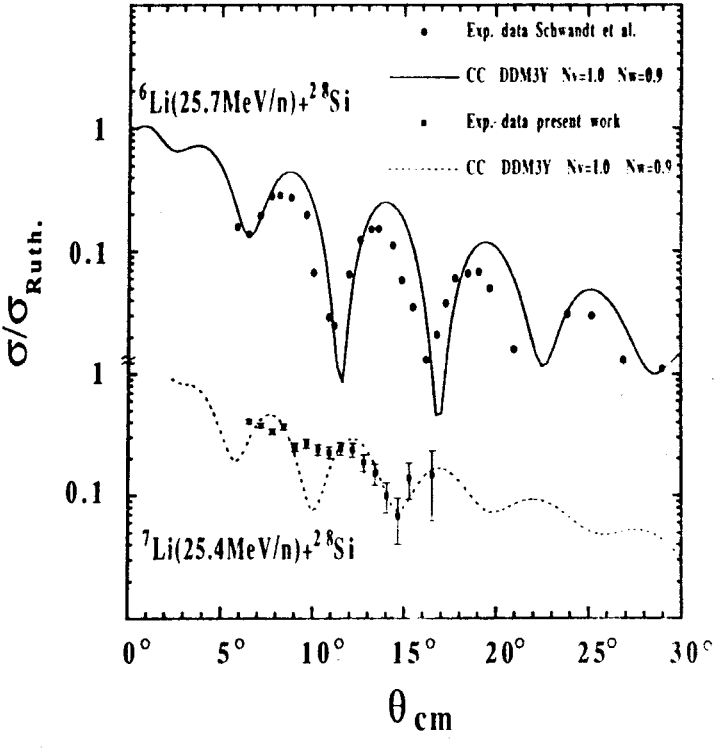

Fig.5. Angular distributions and CC calculation of elastic scattering of light Li isotopes; the bare CC potential is calculated with DDM3Y effective interaction and H.F.-SkII densities; normalization constants are indicated in the figure

lated elastic plus inelastic cross section to the measured one, unreasonably large deformation parameters are needed if the normalization is kept constant at $N_v = 1.0$, $N_W = 1.0$. The calculated reaction cross section for this normalization is about 2 barns for both densities.

Subsequently, one may examine the effect of different choices of ^{11}Li density, as stated above. For the same normalization, the halo density produces a potential with a larger radius (table 3) and the oscillations in the cross section are shifted to smaller angles. As can be seen from figure 6, especially for the large angles the presence of a neutron halo produces a quite different oscillation pattern.

The inability of the presented calculation to reproduce the experimental data leads us to modify the normalization constants. A choice of $N_v = 2.0$, $N_w = 1.0$ gives a reaction cross section of 2 barns, brings the calculated cross

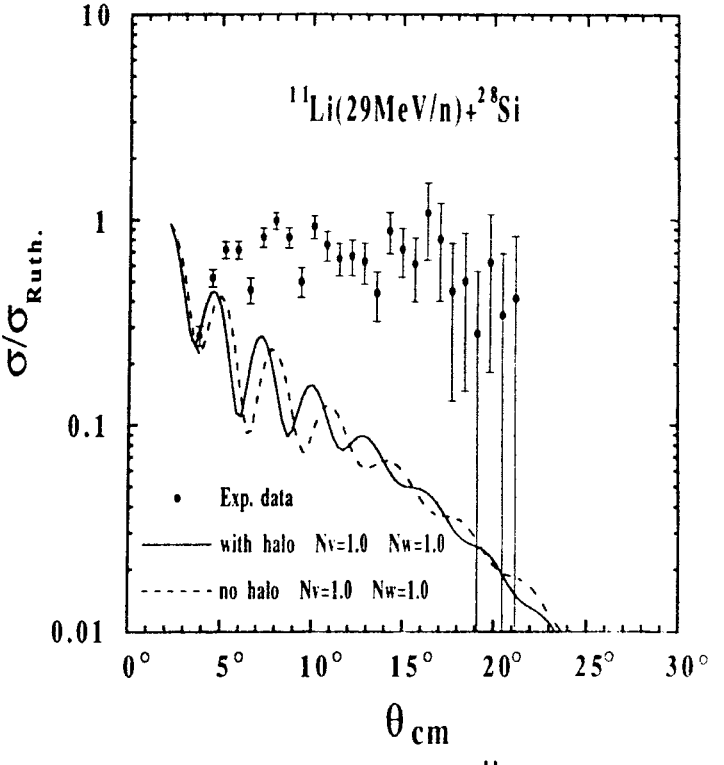

Fig.6. Angular distributions and CC calculation of ^{11}Li elastic scattering; the bare CC double folding potential is calculated with DDM3Y and H.F.–SkII density for ^{28}Si and the halo density of Bertsch et al. [14] for ^{11}Li (solid line) and H.F.–SkII density (dashed line); values of the normalization constants N_v and N_W are indicated in the figure

section over the data, but is unable to reproduce the most prominent oscillations. In order to reproduce the observed oscillations in the data, a reduction in the normalization constants seems to be necessary. The results obtained with $N_v = 0.6$, $N_w = 0.18$ (without neutron halo) and $N_w = 0.27$ (with halo) are shown in figure 7. Different N_w values were taken in order to obtain approximately the same value of the reaction cross section. If the N_w value was equal to 0.18, then the «no halo» calculations give an even smaller reaction cross section, though they come a little closer to the data. While the general trend is reproduced, the reaction cross section drops to a value of 1.4 barn which is quite puzzling in view of the existing data concerning the reaction cross section.

The interaction of ^{11}Li is dominated by the break-up process. In a recent experiment at GANIL [1], the two neutron removal cross section of ^{11}Li on Be (0.47 barn) and Ni (1.3 barn) targets was measured at the same energy as in the present experiment. From these numbers one could esti-

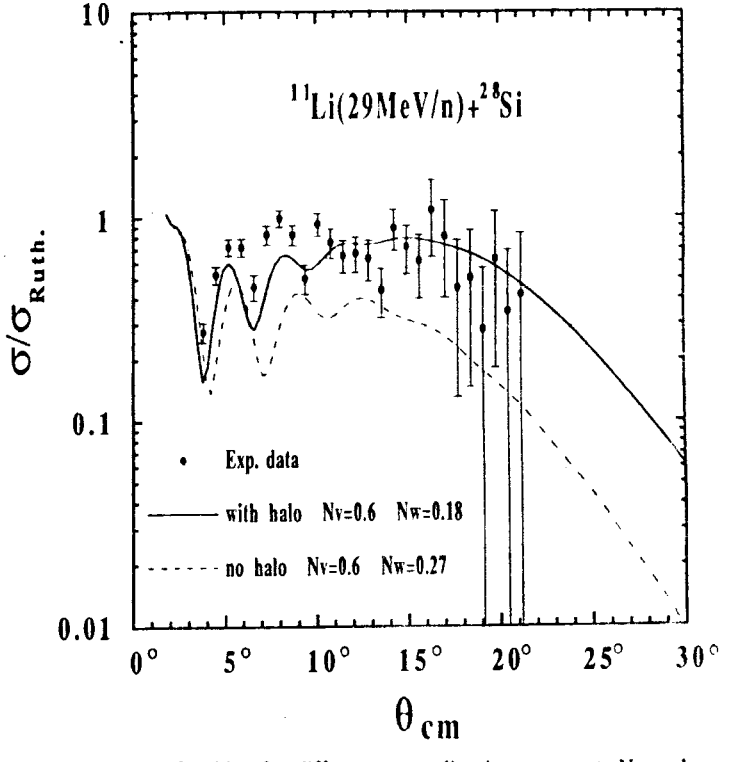

Fig.7. The same as fig.6 but for different normalization constants N_V and N_W; total reaction cross section $\sigma_R = 1.4$ barn in both calculations

mate the break-up cross section for ^{28}Si to be in the range of 0.9—1.0 barn. This is practically one half of the reaction cross section predicted by the formula of Kox et al. [25]. Fukuda et al. [22] have found recently that such empirical formula underpredicts the reaction cross section for halo nuclei by 20—30%. Therefore, a reasonable value of the reaction cross section for $^{11}Li + ^{28}Si$ at 29 MeV/n could be 2.3—2.5 barns, in relative agreement with the value measured by Villari et al. [23] at 25 MeV/n. The measurement of ^{9}Li transverse [3] and parallel [4] momentum distributions showed that due to the very diffuse structure of ^{11}Li, the break-up process is dominant at large impact parameters, in contrast with a «normal» nucleus like ^{7}Li. In the present experiment this is confirmed by the analysis of the energy spectrum of the diffused ^{11}Li ions. If the scattering of ^{11}Li at low impact parameters (i.e. at diffusion angle larger than about 4°) is accompanied by a break-up of this nucleus $^{11}Li \rightarrow {}^{9}Li + 2n$, one should observe in the measured spectum of

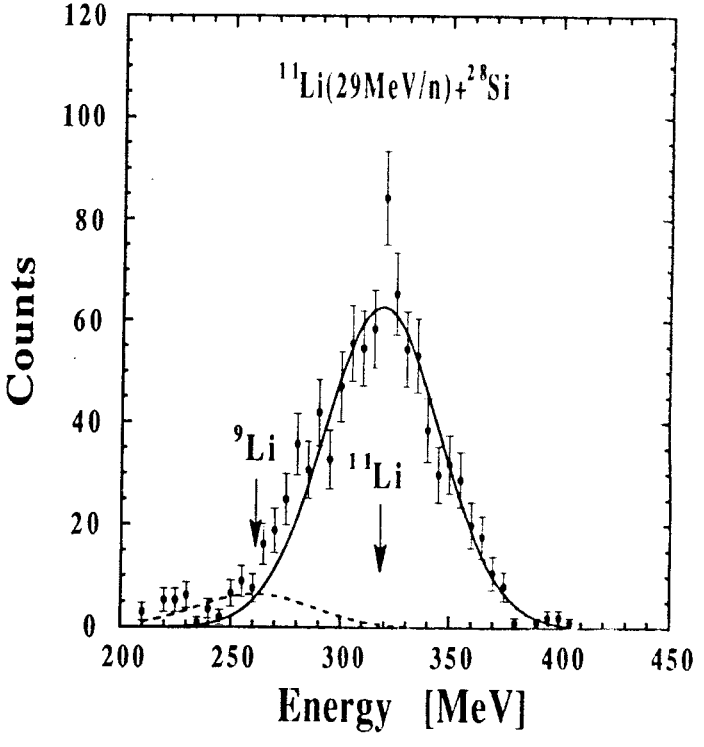

Fig.8. Experimental spectrum of the total energy of scattered ions for the 29 MeV/n ^{11}Li secondary beam; the curves represents a two-gaussian fit centered at the mean energies of ^{9}Li (dashed line) and ^{11}Li (solid line) indicated in the figure by arrows

total energy (sum of energy losses in all detectors), shown in figure 8, a peak corresponding to the 29 MeV/n ^{9}Li ions. A careful mathematical analysis set an upper limit of the contribution of ^{9}Li to 5%. Therefore, the ^{11}Li scattering is influenced by the break-up process only at very small angles, where the optical model amplitude is dominated by the Coulomb scattering. The cross section measured in the angular domain covered by the present experiment is completely insensitive to the break-up process. The loose structure of ^{11}Li is contained in our optical potential through the halo density, which produces only a small shift in the potential radius. A simple renormalization of the potential cannot account for the nonlocal dynamic polarization potential induced by the break-up process. Similar ideas were advanced by Satchler et al. [24]. They suggested that an appropriate normalization of the real folding DDM3Y potential might be equal to 0.57. With this normalization the calculated optical model reaction cross section (1.4 barn) represents approximately the difference between the estimated total reaction cross section and the estimated break-up cross section.

One should also notice that a very similar total reaction cross section (1.45 barn, see table 2) was obtained also in the phenomenological optical model analysis presented in section 4.1.

As can be seen in figure 7 significant differences appear by using different density distributions for ^{11}Li. At practically the same normalization of the effective interaction and at the same total reaction cross section, the halo density reproduces better the data than the no halo density.

5. Conclusions

We have measured for the first time the angular distribution of the elastic scattering of a neutron halo nucleus on the ^{28}Si target. For this purpose, a secondary ^{11}Li beam was used. Despite the rather low intensity, the high efficiency of the detecting system permitted to obtain reliable experimental information. The corresponding angular distribution can be reasonably described by using the phenomenological optical potential and the semimicroscopic double folding model with density and energy dependent effective interaction and realistic densities. However, in the analysis with the phenomenological optical potential the strong modification of the «standard» parameters seems to be necessary for the description of the experimental data. In the semimicroscopic model a strong renormalization of the real part of the optical potential seems to the necessary in order to reproduce the measured angular distributions. At the same time, the important constraint of reproducing the extremely large measured total reaction cross section could not be satisfied. A reason for this discrepancy could be the insensitivity of our data to the break-up process over the measured angular range.

For loosely bound ^{11}Li nucleus, with a very long tail of the neutron density distribution, this process takes place mainly at large impact parameters and the corresponding cross section represents an important fraction of the total reaction cross section. The strong nonlocal dynamical polarization potential induced by this process cannot be simulated by a simple renormalization of the DDM3Y effective interaction.

The results of present experiment confirm conclusions drawn by Kolata et al. [30] on the enhanced refraction and on the importance of a very long absorption in the elastic scattering of ^{11}Li on light targets.

The structure of ^{11}Li enters in the folding potential only through projectile density and the presence of the neutron halo produces relatively small changes in the potential. Nevertheless it seems that the calculations with the halo density reproduce better the experimental data.

Most of the difficulties encountered in the interpretation of the present data come from the lack of separation between elastic and inelastic events which would have required a much better energy resolution for the detected ^{11}Li.

The results of present experiment proved that a measurement of elastic scattering of very exotic nuclei although technically difficult can be performed even at a very low (several hundred particles per second) intensity of a secondary beam. For a complete explanation of the obtained angular and energy distrubiton of diffused ^{11}Li ions particular properties of the ^{11}Li nucleus due to a presence of a neutron halo have to be taken into account. In particular a contribution of soft modes of a giant resonance in ^{11}Li to the elastic cross section is possible and requires further investigations.

Similar experiments performed with higher angular and energy resolution are necessary to confirm and to study the phenomena of neutron halo for other light neutron-rich nuclei as ^{11}Be, ^{14}Be and ^{17}B.

Acknowledgements

We would like to thank Prof. Yu. Oganessian, Dr. N. Alamanos. Dr. R.J. Lombard, Dr. J. Raynal, Dr. K. Terenetsky and Dr. V. Verbitsky for stimulating and fruitful discussions. Furthermore we would like to acknowledge F. Georffroy, R. Hue and A. Latimier for their technical assistance during the experiment. The authors acknowledge the support of the French IN2P3.

References

1. Anne R. et al. — Phys. Lett., 1990, B250, p.19;
   Riisager K. et al. — Nucl. Phys., 1992, A540, p.365.
2. Tanihata I. et al. — Phys. Lett., 1985, 160B, p.380.
3. Kobayashi T. et al. — Proc. Second Int. Conf. on Raioactive Nucl. Beams, Louvain-la-Neuve, Belgium, 19-21 Aug. 1991, ed. Th. Delbar, p.197.

4. Orr N. et al. — To be published;
Morrissey D.J. et al. — Proc. Second Int. Conf. on Radioactive Nuclear Beams, Louvain-la-Neuve, Belgium, 19-21 Aug. 1991, ed. Th. Delbar, p.51.
5. Anne R., Mueller A.C. — Inter. Conf. EMIS-2, Sept. 2-6, 1991, Sendai, Japan, NIM in press and references contained therein.
6. Dlouhy Z. et al. — NIM, in press.
7. Raynal J. — ECIS88, unpublished.
8. Raman S. et al. — At. Data Nucl. Data Tables, 1987, 36, p.1.
9. Nadasen A. et al. — NSCL/MSU Annual Report 1988.
10. Satchler G.R., Love W.G. — Phys. Rep., 1979, 55, p.183.
11. Bertsch G. et al. — Nucl. Phys, 1977, A284, p.399.
12. Kobos A.M. et al. — Nucl. Phys, 1982, A384, p.65;
Kobos A.M. et al. — Nucl. Phys., 1984, A425, p.205;
Brandan M.E., Satchler G.R. — Nucl. Phys., 1988, A487, p.477.
13. Vautherin D., Brink D.M. — Phys. Rev., 1972, C5, p.626.
14. Bertsch G.F., Brown B.A., Sagawa H. — Phys. Rev., 1989, C39, p.1154.
15. Tanihata I. et al. — Phys. Lett., 1988, B206, p.592.
16. Schwandt P. et al. — Phys,. Rev., 1980, C21, p.1656.
17. Satchler G.R. — Phys. Rev., 1980, C22, p.919.
18. Tiede M.A., Trcka D.E., Kemper K.W. — Phys. Rev., 1991, C44, p.1698.
19. Sakuragi Y. — Phys. Rev., 1987, C35, p.2161.
20. Yamagata T. et al. — Phys. Rev., 1989, C39, p.873.
21. Saint-Laurent M-G. — Z. Phys., 1989, A332, p.457.
22. Fukuda M. et al. — Phys. Lett., 1991, B268, p.339.
23. Villari A.C.C. — Phys. Lett., 1991, B268, p.345.
24. Satchler G.R., McVoy K.W., Hussein M.S. — Nucl. Phys., 1991, A522, p.621.
25. Kox S. et al. — Phys. Rev., 1987, C35, p.1678.
26. Cook J. — Nucl. Phys., 1982, A388, p.153.
27. Nadasen A. et al. — Phys. Rev., 1989, C39, p.536.
Nadasen A. et al. — Phys. Rev., 1989, C40, p.1237.
28. Zisman M.S. et al. — Phys. Rev., 1980, C21, p.2398.
29. Moon C.B. et al. — Preprint RIKEN-AF-NP-126, to be published.
30. Kolata J.J. et al. to be published.
31. Fuller R.C. — Phys. Rev., 1975, C12, p.1561.
32. Dem'yanova A.S. et al. — Nucl. Phys., 1989, A501, p.336.
33. Fayans S.A. — Phys. Lett., 1991, B267, p.443.

Received on October 26, 1992.